Activation of water on MnO$_x$-modified rutile (110) and anatase (101) TiO$_2$ and the role of cation reduction.

Stephen Rhatigan and Michael Nolan*

Tyndall National Institute, University College Cork, Lee Maltings, Cork, Ireland

michael.nolan@tyndall.ie

Abstract

Surface modification of titania surfaces with dispersed metal oxide nanoclusters has the potential to enhance photocatalytic activity. These modifications can induce visible light absorption and suppress charge carrier recombination which are vital in improving the efficiency. We have studied heterostructures of Mn$_4$O$_6$ nanoclusters modifying the TiO$_2$ rutile (110) and anatase (101) surfaces using density functional theory corrected for on-site Coulomb interactions (DFT + U). Such studies typically focus on the pristine surface, free of the point defects and surface hydroxyls present in real surfaces. In our study we have considered partial hydroxylation of the rutile and anatase surfaces and the role of cation reduction, via oxygen vacancy formation, and how this impacts on a variety of properties governing the photocatalytic performance such as nanocluster adsorption, light absorption, charge separation and reducibility. Our results indicate that the modifiers adsorb strongly at the surface and that modification extends light absorption into the visible range. MnO$_x$-modified anatase can show an off-stoichiometric ground state, through oxygen vacancy formation and cation reduction spontaneously, and both modified rutile and anatase are highly reducible with moderate energy costs. Manganese ions are therefore present in a mixture of oxidation states. Photoexcited

1

electrons and holes localize at cluster metal and oxygen sites, respectively. The interaction of water at the modified surfaces depends on the stoichiometry and spontaneous dissociation to surface bound hydroxyls is favoured in the presence of oxygen vacancies and reduced metal cations. Comparisons with bare TiO_2 and other TiO_2-based photocatalyst materials are presented throughout.

Introduction

Photocatalysts are semiconductor materials which absorb photons of energies in excess of the bandgap to produce electron-hole pairs. These charge carriers separate and migrate to the surface of the catalyst where they drive chemical reactions *via* reduction and oxidation of adsorbed species. Photocatalysis has a variety of applications, including, but not limited to, the solar production of hydrogen from water splitting.[1; 2; 3; 4]

A practical photocatalyst must meet a number of criteria, such as visible light absorption, efficient charge carrier separation, stability and active surface sites for the adsorption of feedstock species. Reducible metal cations in the catalyst can be important for enhancing the activity of the catalyst towards the difficult step of water dissociation. The development of metal oxide photocatalysts is of interest as these materials are cheap, earth abundant and, in many instances, non-toxic. Indeed, the most widely studied photocatalyst is titanium dioxide (TiO_2)[2; 3; 5; 6; 7; 8; 9] which was first demonstrated as a photoanode for water splitting by Fujishima and Honda in 1972.[10] The large bandgap (> 3 eV) means that photoactivity is restricted to the UV and has limited the real-world application of TiO_2-based photocatalyst technologies. As a result, significant scientific effort has focused on extending the light absorption edge of TiO_2 to longer wavelengths.

Substitutional doping of TiO_2 with cations and/or anions is a widely studied approach to inducing visible light absorption through the emergence of impurity-derived energy levels in

the TiO_2 bandgap.[8; 11; 12; 13; 14; 15; 16; 17; 18; 19; 20; 21; 22; 23; 24; 25; 26; 27; 28] First principles studies of such doped systems typically focus on bandgap reduction[13; 22; 25; 26; 29; 30; 31; 32] and questions of charge localization and surface reactivity are often overlooked. These are important considerations as dopant-derived defect states have been shown to act as recombination centres[8; 18; 21] and photocatalysis is generally a surface mediated phenomenon.

Studies of the chemistry and electronic properties of surfaces and interfaces are key to understanding and screening materials for photocatalysis. The enhanced performance of the benchmark material, P25, which consists of chemically interfaced rutile and anatase phases, has been attributed to the favourable alignment of the conduction and valence bands at the interface which facilitates charge transfer between phases and the suppression of charge carrier recombination.[33] In addition, the interface can promote the formation of active catalytic sites. This effect can be tuned by considering heterostructures with metal oxides of different compositions. Such heterostructures have been realised experimentally and shown to exhibit enhanced photocatalytic activity.[34; 35; 36; 37; 38] Nanostructuring of metal oxides has been investigated as an approach to enhancing charge transfer kinetics and increasing surface area while providing low-coordinated metal and oxygen sites for the adsorption of feedstock species.[39; 40; 41; 42] Further, nanostructuring can also facilitate the reduction of metal cations.

Surface modification of metal oxide surfaces with dispersed metal oxide nanoclusters combines the properties of hetero- and nano-structuring. Sub-nm nanoclusters of iron oxide were deposited on TiO_2 surfaces *via* chemisorption-calcination cycle (CCC)[9; 43] and atomic layer deposition (ALD).[44] FeO_x-modified TiO_2 exhibited bandgap reduction and enhanced visible light photocatalytic activity. The modification was shown to suppress carrier recombination as indicated by photoluminescence spectroscopy.[43] The red-shift in light absorption was

3

attributed to cluster-derived states above the valence band maximum (VBM) which were identified by X-ray photoelectron spectroscopy (XPS) and density functional theory (DFT) simulations.[9; 43; 45]

These studies, and the subsequent development of similar systems,[37; 46; 47; 48; 49] mean that a multitude of nanocluster-surface composites can be investigated. Considerations for tuning these systems for optimal performance include composition, surface termination, nanocluster size, and stoichiometry; all of which contribute to the light absorption properties, charge carrier mobility and surface reactivity. DFT simulations can be used to illuminate the properties underpinning experimental observations[45; 47; 48; 50] and to screen candidate materials worthy of further investigation.[51; 52; 53; 54; 55; 56; 57; 58; 59; 60; 61]

In the present study we use first principles DFT calculations to examine the photocatalytic properties of manganese oxide modified TiO_2, using model systems of Mn_4O_6-nanoclusters modifying the rutile (110) and anatase (101) surfaces and consider the role of partial surface hydroxylation in the interfacial chemistry. Our analysis includes an assessment of the stability of the composite surfaces, their ground state stoichiometry and reducibility *via* oxygen vacancy formation. Point defects, such as oxygen vacancies, are active sites at metal oxide surfaces and can be produced thermally. A more reducible surface will lose oxygen more readily and be more active in solar thermal[62] or Mars van Krevelen processes.[63; 64] Computed density of states plots elucidate the impact of modification on the light absorption properties and a model for the photoexcited state[65] is used to examine charge separation and localization. Finally, we study the interaction of water with the modified surfaces and focus particularly on the role of oxygen vacancies and reduced cations on water adsorption. We identify the characteristics of activation, such as dissociation, geometry distortions and charge transfer to the adsorbed species. The importance of oxygen vacancies as active sites for water dissociation at the rutile (110) surface[66; 67] and ceria surfaces[68] has been widely discussed and reduced

4

Ti^{3+} ions have been shown to be active in the chemistry at titania surfaces.[69; 70] For anatase TiO$_2$, oxygen vacancies have been shown to be more stable at subsurface and bulk sites than on the surface.[71; 72] However the surface can be reduced by electron bombardment[72; 73] and the reaction of these vacancy sites with water and O$_2$ results in water dissociation. These studies highlight the necessity of engineering photocatalytic surfaces for which vacancies can be produced with moderate energy costs.

MnO$_x$ is an interesting modifier as manganese is a multi-valent, reducible element which crystallizes in oxides with a variety of oxidation states;[74] this will have implications for the light absorption properties and reducibility of sub-nm nanoclusters of MnO$_x$ dispersed at the titania surfaces. We have previously studied similar systems of MnO$_x$-modified TiO$_2$, in collaboration with experiment, to interrogate their activity for CO$_2$ capture and reduction.[75] The Mn$_4$O$_6$-TiO$_2$ composites were found to be stoichiometric in the ground state for both modified rutile and anatase, albeit with moderate costs to produce reducing oxygen vacancies (+0.59 eV for rutile and +1.1 eV for anatase). However, the impact of surface hydroxyls on the formation of oxygen vacancies was not fully investigated; we show that vacancy formation is in fact promoted with hydroxyls present at the TiO$_2$ surfaces. The photoexcited state model, which examines localization of electrons and holes at nanocluster metal and oxygen sites, sheds light on experimental observations which suggest that the MnO$_x$-modifiers may facilitate recombination.[75] In addition, active oxygen vacancy sites play a crucial role in the subsequent interaction of water molecules and their adsorption modes. In particular, dissociation is favoured for the reduced systems; this is an important step in the water oxidation reaction.

Methodology

Periodic plane wave DFT calculations are performed using the VASP5.2 code[76; 77] with an energy cut-off of 400 eV. The core-valence interaction is described with projector augmented wave (PAW) potentials[78; 79], with 4 valence electrons for Ti, 6 for O, 13 for Mn and 1 for H species. The Perdew-Wang (PW91) approximation to the exchange-correlation functional is used.[80]

The TiO_2 rutile (110) and anatase (101) substrates are modelled as 18 and 12 atomic layer slabs, respectively, with (2×4) surface expansions and vacuum gaps of 20 Å, as used in our previous studies.[53; 54; 61; 75; 81] Γ-point sampling is used and the convergence criteria for the energy and forces are 10^{-4} eV and 0.02 eVÅ^{-2}, respectively. All calculations are spin polarized.

A Hubbard U correction is implemented to consistently describe the partially filled Mn 3d states and reduced Ti^{3+} states.[82; 83] The values of U used are U(Ti) = 4.5 eV and U(Mn) = 4 eV and these have been chosen based on previous work on TiO_2[45; 46; 53; 81; 84; 85; 86] and manganese oxides.[74; 87]

To model surface hydroxylation (before the nanoclusters are adsorbed) and the impact on the heterostructure chemistry, four water molecules are dissociatively adsorbed at the clean rutile (110) and anatase (101) surfaces which gives a partial coverage of 50%. The hydroxylated surfaces are denoted by OH-r110 and OH-a101. These models are representative of hydroxylated rutile and anatase surfaces, while we are not attempting to describe the most stable solutions for water or dissociative water adsorption at these titania surfaces.[46; 53; 81]

The Mn_4O_6 nanocluster (see *Supporting Information*) was adsorbed in different configurations at the hydroxylated rutile (110) and anatase (101) surfaces and the adsorption energies are computed using:

$$E_{ads} = E_{surf+A} - E_{surf} - E_A \tag{1}$$

where E_{surf+A}, E_{surf} and E_A are the energies of the adsorbate-surface composite system, the hydroxylated titania surface and the gas phase nanocluster respectively.

For the reduction of the composite surface, each of the six O sites of the supported nanocluster is considered for the formation of an oxygen vacancy, O_V. One oxygen ion is removed from the Mn_4O_x cluster and the vacancy formation energy is calculated as:

$$E_{vac} = E(Mn_4O_{x-1}) + 1/2E(O_2) - E(Mn_4O_x) \tag{2}$$

where the first and third terms on the right hand side are the total energy of the cluster-surface composite with and without an oxygen vacancy and the energy is referenced to half the total energy for molecular O_2. Having identified the most stable structure with a single O_V, the calculation is repeated for each of the five remaining O sites to determine the most stable structure with two O_V. Oxidation states are investigated with Bader charge analysis and computed spin magnetizations.

We apply a model for photoexcitation to the ground state configuration of each modified surface and to the unmodified OH-r110 and OH-a101 surfaces for comparison. This model involves imposing a triplet electronic state on the system[65] to promote an electron to the conduction band, with a corresponding hole in the valence band. The analysis of the energies and charge localization is discussed in more detail in the *Supporting Information.*

For the interaction of water with the modified surfaces, H_2O molecules are adsorbed in various configurations at the oxygen deficient systems and the adsorption energies are calculated as:

$$E_{ads} = E_{surf+H_2O} - E_{surf} - E_{H_2O} \tag{3}$$

where E_{surf+H_2O}, E_{surf} and E_{H_2O} refer to the energies of the H_2O molecule and modified surface in interaction, the modified surface, and the gas phase H_2O, respectively.

Oxygen atoms of the surface, cluster and surface bound hydroxyls are denoted O_S, O_C and O_{OH}, respectively, and similar notation is adopted for OH groups. For the interaction of water with the modified surfaces, water-derived oxygen and hydroxyls are denoted O_W and OH_W.

Results

Stoichiometric Mn₄O₆-modified TiO₂ OH-rutile (110) and OH-anatase (101).

Figures 1(a) and 1(b) show the adsorption energies and relaxed atomic structures of the stoichiometric Mn_4O_6-nanocluster modifying the OH-r110 and OH-a101 surfaces. The large, negative adsorption energies indicate that the nanocluster-surface interaction is favourable and that the nanoclusters will be stable against desorption and aggregation.[53; 54; 60; 61; 81; 88] For Mn_4O_6-OH-r110 (Figure 1(a)), three Mn ions are four-fold coordinated and to each of these is bound a terminal OH. Of these OH groups, one has migrated from a Ti site in the rutile surface to an Mn ion of the cluster (OH_{OH}) and two OH groups result from the migration of hydrogen from surface hydroxyls to O_C atoms (OH_C). The fourth Mn ion is five-fold coordinated and is bound to three O_C and two O_S ions (one bridging O_S and one in-plane O_S). Five O ions of the OH-r110 surface bind with Mn of the nanocluster (three O_S and two O_{OH}) and two O_C ions bind to Ti of the surface. Mn-O distances are in the range 1.8-2.1 Å; the shorter distances involve two-fold coordinated O ions and for Mn bound to the in-plane O_S ion the Mn-O distance is 2.2 Å. Ti ions which bind to the nanocluster migrate out from the surface by 0.1 Å, however, distortions to the geometry of the rutile (110) surface are minimal.
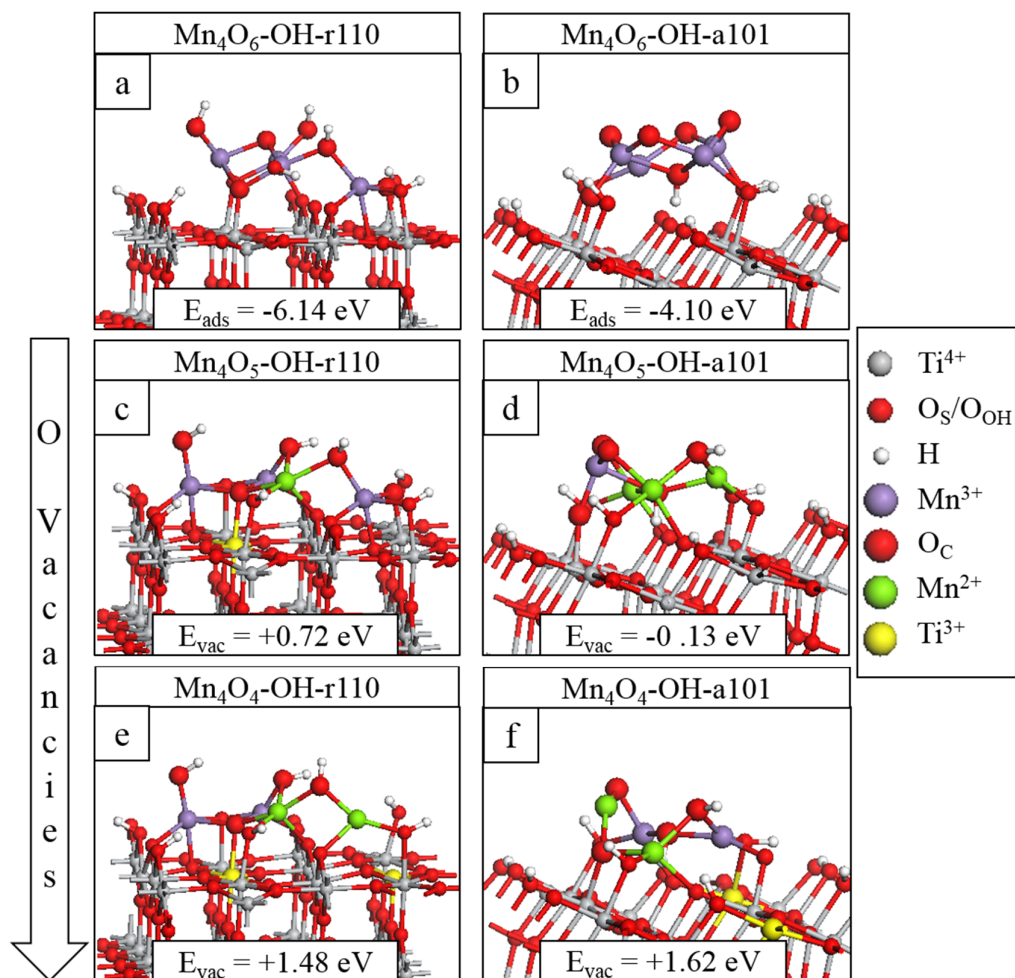
Figure 1 Relaxed atomic structures of Mn_4O_x modifying the hydroxylated titania surfaces. The stoichiometric composites are shown in **(a)** for Mn_4O_6-OH-r110 and **(b)** for Mn_4O_6-OH-a101; the nanocluster adsorption energies are included in the inset. The atomic structures after formation of the most stable single O_V are shown in panels **(c)** for Mn_4O_5-OH-r110 and **(d)** for Mn_4O_5-OH-a101. The atomic structures of the most stable composites with two O_V are shown in panels **(e)** for Mn_4O_4-OH-r110 and **(f)** for Mn_4O_4-OH-a101. The energy costs to produce O_V are included and computed relative to the structure with one less O_V. Atomic species and oxidation states are indicated by the colours in the legend on the right hand side.

For Mn_4O_6-OH-a101 (Figure 1(b)), three Mn ions are four-fold coordinated and one Mn is three-fold coordinated. Five O_C sites are two-fold coordinated with one O_C ion binding to three Mn ions and a H atom which has migrated from a bridging O_S site. Of the four interfacial bonds between the Mn_4O_6 nanocluster and OH-a101, three involve Mn and OH_{OH} groups; the fourth is a Ti-O_C bond. Mn-O distances are in the range 1.7-2.1 Å.

9

For Mn_4O_6 adsorbed at OH-r110, the computed Bader charge for each of the Mn is in the range 11.2-11.3 electons, typical of Mn^{3+} ions (see Table 1). The spin magnetizations for these sites are each 3.9 μ_B, which reflects the $3d^4$ configuration of the Mn^{3+} ion.

For the Mn_4O_6 nanocluster adsorbed at OH-a101, two Mn ions are reduced to Mn^{2+}. The computed Bader charges for these sites are 11.5 electrons, compared to 11.3 electrons for Mn^{3+} ions (see Table 1). The corresponding spin magnetizations are 4.6 μ_B on these sites, while on the Mn^{3+} sites, the spin magnetisations are 3.1-3.3 μ_B for modified OH-a101. In this heterostructure, the accumulation of negative charge at these Mn sites is accompanied by a more positive charge on the O_C sites, which have Bader charges of 7.0 electrons, compared to 7.2-7.7 electrons for O^{2-} anions.

Table 1 Computed Bader charges for the manganese ions in the supported nanoclusters before and after formation of one or more O_V. Also included are Bader charges for titanium ions of the support which are reduced after vacancy formation. Reduced Mn^{2+} and Ti^{3+} are highlighted in bold.

Surface	OH-r110				OH-a101		
Modifier	Mn_4O_6	Mn_4O_5	Mn_4O_4		Mn_4O_6	Mn_4O_5	Mn_4O_4
Mn_I	11.3	11.3	**11.5**	Mn_I	**11.5**	**11.5**	11.3
Mn_{II}	11.3	11.3	11.3	Mn_{II}	**11.5**	**11.5**	**11.5**
Mn_{III}	11.2	**11.5**	**11.5**	Mn_{III}	11.2	**11.5**	11.3
Mn_{IV}	11.3	11.3	11.3	Mn_{IV}	11.2	11.2	**11.6**
Ti_I	1.3	**1.7**	**1.7**	Ti_I	1.3	1.3	**1.7**
Ti_{II}	1.3	1.3	**1.7**	Ti_{II}	1.3	1.3	**1.7**

Reduction of Mn_4O_6-modified TiO_2 OH-rutile (110) and OH-anatase (101) via oxygen vacancy formation.

The most stable modified surfaces with a single O_V are shown in Figure 1(c) for Mn_4O_5-OH-r110 and Figure 1(d) for Mn_4O_5-OH-a101. For the modified OH-r110 surface the formation

energy of a single O_V is +0.72 eV (vacancy formation energies for other sites of the nanocluster were in the range 1.4-1.9 eV). This formation energy is moderate and suggests that O_V could be easily produced under moderate experimental conditions. After formation of the most stable vacancy, three Mn ions are five-fold coordinated and the fourth Mn cation is four-fold coordinated. Four bridging and two in-plane surface oxygen are bound to Mn ions of the nanocluster. Two O_C ions bind to surface Ti sites while three O_C ions are bound only to Mn and H ions. The formation of the neutral oxygen vacancy releases two electrons. The Bader charge analysis reveals that these localize at a five-fold coordinated surface Ti site and an Mn site of the nanocluster. The computed Bader charges on this Ti site increases from 1.3 to 1.7 electrons and on the Mn site, the Bader charge is 11.5 electrons; see Table 1 for computed Bader charges of reduced Ti and all Mn sites. The computed spin magnetizations are 1.0 μ_B and 4.6 μ_B for Ti and Mn. These values are typical of the formation of reduced Ti^{3+} and Mn^{2+} ions.

For the modified OH-a101 surface, the most stable O_V has a formation energy of -0.13 eV which indicates that it will spontaneously form, so that the ground state is off-stoichiometric (vacancy formation energies for other sites of the nanocluster were in the range 0.1-2.0 eV). This compares with Mn_4O_6 modifying bare anatase (101) which was found to be stoichiometric in the ground state.[75] After the formation of this O_V, two Mn ions relax towards the titania surface and bind with bridging O_S sites so that, in this configuration, each of the Mn ions is four-fold coordinated. Bader charge analysis and computed spin densities indicate that three Mn ions are reduced to Mn^{2+}, having computed Bader charges of 11.5 electrons and computed spin magnetisations of 4.6 μ_B. The two electrons released by O_V formation reduce one Mn cation to Mn^{2+} and the second electron is donated to a nanocluster oxygen, for which the Bader charge and spin magnetization are 7.6 electons and 0.0 μ_B, compared to values of 7.0 electrons

and 0.2 μ_B in stoichiometric Mn_4O_6-OH-a101. That O_V formation is more facile for modified anatase corroborates previous experimental work on MnO_x-TiO_2.[75]

The formation of the second O_V has a moderate energy cost for both MnO_x-modified TiO_2 surfaces. The most stable configurations of the heterostructures with two O_V are shown in Figure 1(e) for Mn_4O_4-OH-r110 and Figure 1(f) for Mn_4O_4-OH-a101. For the Mn_4O_4-OH-r110 surface, the most stable O_C site for formation of a second O_V was two-fold coordinated to a cluster Mn and surface Ti ion. After vacancy formation the Mn ion moves away from the surface, breaking a bond with an in-plane O_S ion and becomes three-fold coordinated, having been originally five-fold coordinated. The Bader charge and spin magnetization for this site are 11.5 electrons and 4.6 μ_B, respectively. Similarly, for the Ti site to which the removed O_C was bound, the Bader charge and spin magnetization are 1.7 electrons and 1.0 μ_B. Hence, the Mn_4O_4-OH-r110 heterostructure with two oxygen vacancies has two Ti^{3+} and two Mn^{2+} ions.

For the modified OH-a101 surface, a two-fold coordinated O_C site, bridging two Mn ions, has the lowest cost to produce a second O_V. One Mn ion that was bound to the removed O_C atom is two-fold coordinated, having been originally coordinated to four O_C ions. The second Mn ion remains four-fold coordinated. In this Mn_4O_4-OH-a101 configuration, there are two Ti^{3+} and two Mn^{2+} ions, similarly to Mn_4O_4-OH-r110, with computed Bader charges of 11.5 and 1.7 electrons and spin magnetizations of 4.6 and 1.0 μ_B, on Mn and Ti, respectively.

The localization of electrons at Ti and Mn sites is also accompanied by localised geometry distortions. The cation-O distances increase by ~0.1 Å after reduction, reflecting the larger ionic radii of Mn^{2+} and Ti^{3+} compared to Mn^{3+} and Ti^{4+}.[89]

Electronic properties of Mn_4O_x-modified TiO_2 OH-rutile (110) and OH-anatase (101).

The top panels of Figure 2 show the projected electronic density of states (PEDOS) of Mn_4O_6-modified OH-r110 for (a) the stoichiometric ground state and the reduced states with (b) one

and (c) two O_V. The PEDOS plots show that occupied nanocluster-derived states (Mn 3d and O_C 2p) extend to 0.3, 0.4 and 0.55 eV above the valence band maximum (VBM) of the rutile support for Mn_4O_6-, Mn_4O_5- and Mn_4O_4-OH-r110, respectively. Unoccupied Mn 3d-derived states also emerge in the titania band gap at 0.4, 0.25 and 0.2 eV below the conduction band minimum (CBM) for the stoichiometric ground state and the reduced states with one and two O_V. Additional states emerge in the band gap due to occupied Ti^{3+} states (see insets of Figures 2(b) and (c)), for the composites with one and two O_V.
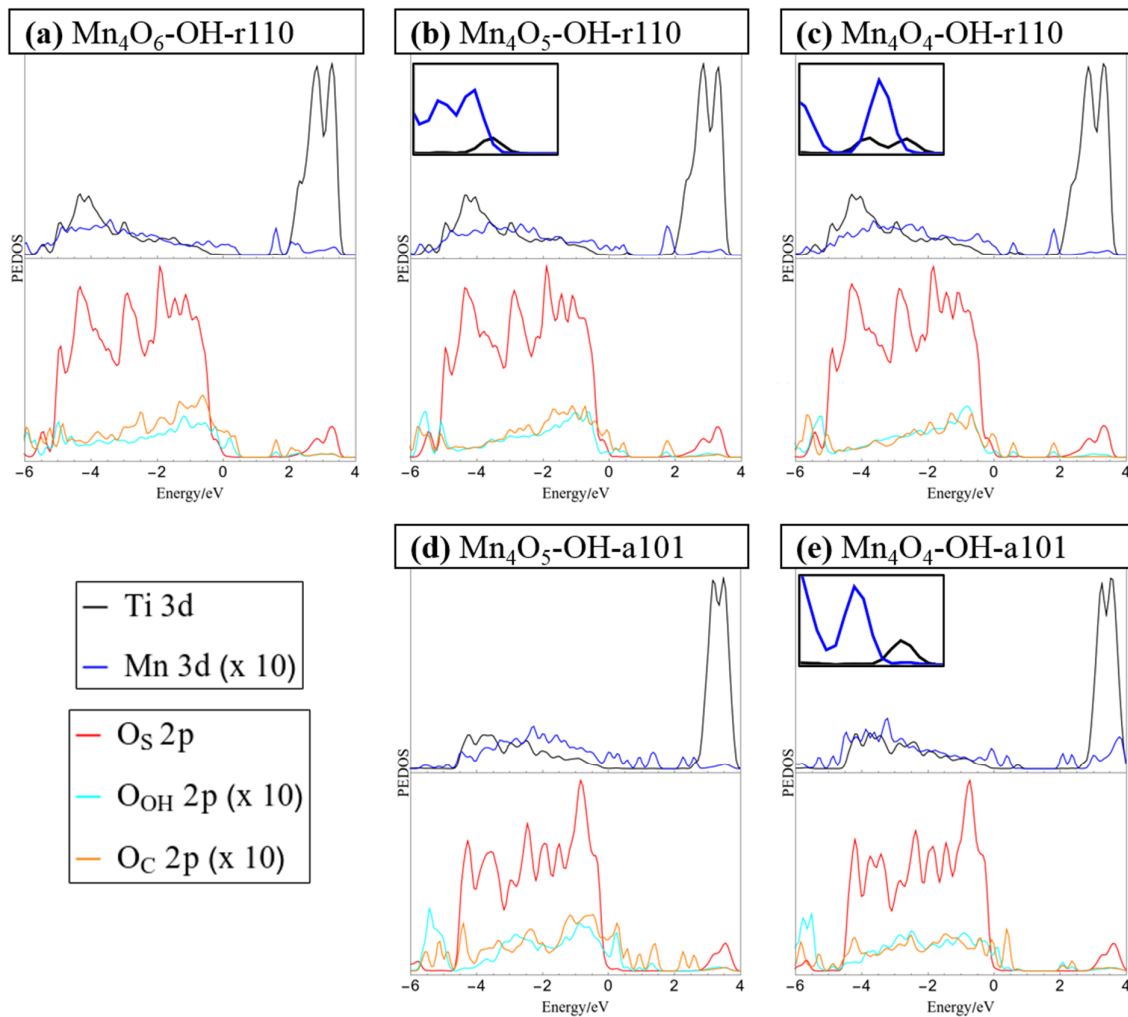

Figure 2 Projected electronic density of states (PEDOS) plots for **(a)** Mn_4O_6-, **(b)** Mn_4O_5-, and **(c)** Mn_4O_4-OH-r110 and **(d)** Mn_4O_5-, and **(e)** Mn_4O_4-OH-a101. The TiO_2 VBM is set to 0 eV. The top half of each panel displays Ti and Mn 3d derived states. The bottom halves of the panels show contributions to the DOS from oxygen 2p states of the surface (O_C), surface bound hydroxyls (O_{OH}) and nanocluster (O_C). Insets in panels **(b)**, **(c)** and **(e)** show the mid-gap occupied Ti 3d states in the range [0 eV, 1 eV].

The bottom panels of Figure 2 display the PEDOS of the modified OH-a101 surface for (d) the ground state, with one O_V, and (e) reduced state with two O_V. Since this heterostructure is off-stoichiometric in the ground state, the PEDOS plot for Mn_4O_6-OH-a101 has been omitted from this figure, and is included in the *Supporting Information* for completeness. The PEDOS plot for the ground state, with one O_V, shows that occupied Mn 3d- and O_C 2p-derived states extend to 1.4 eV above the titania derived VBM, while unoccupied Mn 3d states emerge at 0.5 eV below the CBM, leading to a significant reduction in the computed energy gap relative to TiO_2. For the reduced structure, with two O_V, the highest occupied state is that resulting from Ti^{3+} formation which lies higher in energy by 0.7 eV relative to the VBM of the anatase support (see inset of Figure 2(e)). The lowest energy, unoccupied state is Mn-derived and is 0.8 eV below the CBM. For Mn_4O_4-OH-a101 the energy gap is 1.2 eV, with our DFT+U set-up showing a reduction over unmodified anatase.

These features of the PEDOS for Mn_4O_x-TiO_2 can be attributed to formation of interfacial bonds, the presence of low-coordinated Mn and O_C sites and the facile formation of O_V in the supported metal oxide nanocluster. Modification pushes the VBM to higher energy and results in the emergence of empty states below the CBM; these effects, and the consequent red shift, are greater for modified anatase, consistent with previous reports.[75] These metal oxide nanocluster-modified surfaces are of interest for the oxygen evolution half reaction (OER) of the water splitting process and in this context raising the VBM from that of TiO_2 and towards the water oxidation potential is a desirable effect. Lowering of the titania CBM from its favourable position straddling the water reduction potential is detrimental to the hydrogen evolution reaction (HER) activity. However, as H adsorbs too strongly at metal oxide surfaces, such heterostructures will in any case not be suitable photocathodes for water splitting.

14

Photoexcitation model

We apply the model for the photoexcited state to the ground state systems, Mn_4O_6-OH-r110 and Mn_4O_5-OH-a101. Table 2 presents the computed vertical, singlet-triplet and electron-hole trapping energies, as discussed in the *Supporting Information.* As can be seen from the values listed in Table 2, the underestimation of the bandgap inherent in approximate DFT is present in our DFT+U computational set-up. Our goal in choosing +U corrections is to consistently describe the localization of electrons and holes rather than reproduce the bandgap of bulk TiO_2, which is not advised. Comparison of these computed energies across different structures nonetheless yields useful qualitative information about the effect of surface modification and results for the unmodified OH-r110 and OH-a101 surfaces are included for reference. In particular, $E^{vertical}$ is analogous to the optical band gap, and a reduction in this value for a heterostructure relative to unmodified titania implies that modification leads to a red shift in light absorption.

Table 2 Vertical singlet-triplet energy difference ($E^{vertical}$), the relaxed singlet-triplet energy difference (E^{excite}) and the relaxation energy (E^{relax}) for Mn_4O_6-OH-r110 and Mn_4O_5-OH-a101. Values for hydroxylated rutile (110) and anatase (101) surfaces have been included for reference.

Composite structure	$E^{vertical}$ (eV)	E^{excite} (eV)	E^{relax} (eV)
OH-rutile (110)	2.02	1.47	0.55
Mn_4O_6-OH-rutile (110)	1.48	0.27	1.21
OH-anatase (101)	2.69	1.39	1.30
Mn_4O_5-OH-anatase (101)	1.51	0.42	1.09

When comparing Mn_4O_6-OH-r110 with unmodified OH-r110 and Mn_4O_5-OH-a101 with unmodified OH-a101, decreases in $E^{vertical}$ by 0.54 and 1.18 eV, respectively, indicate that modification leads to a significant red shift in light absorption in both instances. These results corroborate the analysis of the PEDOS. E^{relax} is the energy gained by the system after structural

relaxation in response to the triplet electronic state and is related to the stability of the trapped electron and hole. The relaxation energy is larger for Mn_4O_6-OH-r110 than that computed for unmodified OH-r110 and reflects the greater flexibility of the modified system in accommodating the triplet electronic state. The relaxation energies for Mn_4O_5-OH-a101 and unmodified OH-a101 are comparable. The mixture of Mn oxidation states at the anatase surface restricts the degree to which the nanocluster can respond structurally to the localization of photoexcited charges.
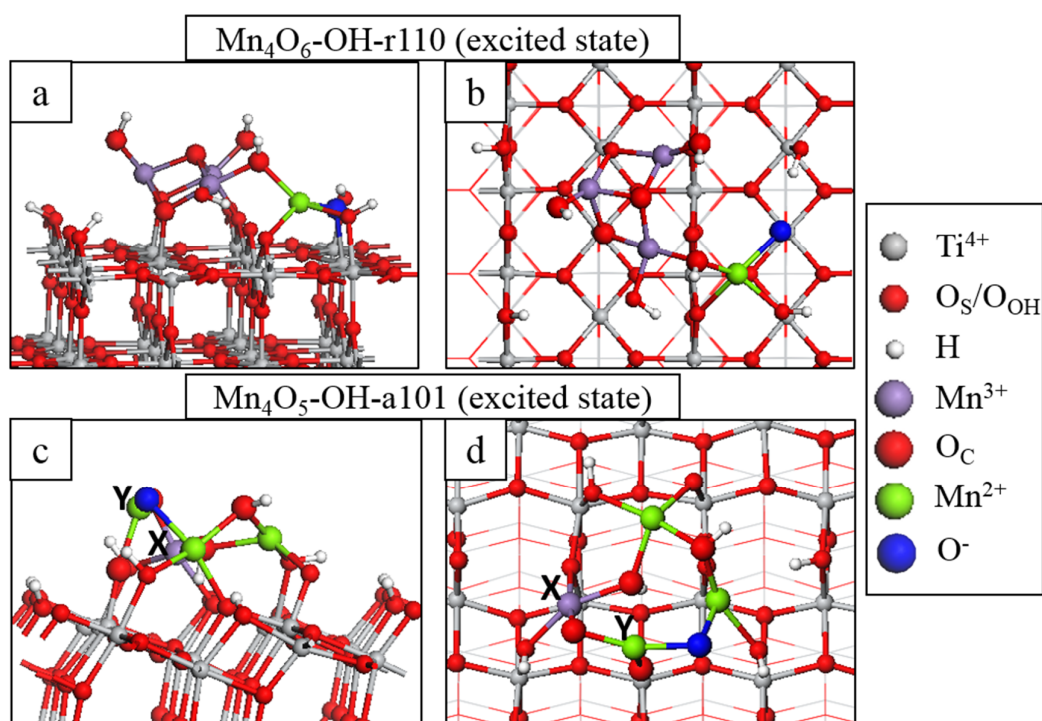

Figure 3 Atomic structure of the fully relaxed triplet electronic state imposed on Mn_4O_6-OH-r110 for **(a)** side and **(b)** top view and Mn_4O_5-OH-a101 for **(c)** side and **(d)** top view. Charge localization and changes in oxidation state are distinguished by colour according to the legend on the right hand side.

Through analysis of Bader charges and spin magnetizations we can determine the electron and hole localization sites and the results of this analysis are represented graphically in Figure 3. For Mn_4O_6-OH-r110, in Figure 3(a) and (b), the electron localizes at an Mn site; the Bader

charge and spin magnetization for this site are 11.5 electrons and 4.6 μ_B after electron localization, which are typical of Mn^{2+} formation. The hole localizes at an O_C site which is two-fold coordinated to the Mn^{2+} ion and a surface Ti. In this instance the Bader charge is 6.8 electrons and the spin magnetization is 0.8 μ_B, which are consistent with formation of O^-. The Mn^{2+}-O^- distance increases by 0.2 Å, relative to the ground state. The Ti-O^- distance decreases by 0.1 Å.

For Mn_4O_5-OH-a101 in the ground state there are three Mn^{2+} ions as discussed above. In the excited state (Figure 3(c) and (d)), there are still three Mn^{2+} ions, however, their distribution is changed. Looking at Figure 3(c) and (d), and comparing with Figure 1(d), we can see that an electron hops from the Mn site indicated with **X** in the ground state to the Mn site indicated with **Y** after imposition of the triplet state. The latter Mn cation was originally four-fold coordinated in the ground state and after electron localisation is three-fold coordinated, whereby a bond to the central O_C site is broken. Formation of Mn^{2+} at this site is confirmed by a computed Bader charge of 11.6 electrons and spin magnetization of 4.6 μ_B. The hole state localizes predominantly at an O_C site which bridges two Mn^{2+} ions. After hole localization the Bader charge is 6.7 electrons and the spin magnetization is 0.8 μ_B. The Mn^{2+}-O distances increase by 0.2-0.3 Å.

These results show that the electron localizes at an Mn site of the supported nanocluster and the hole state localizes at a neighbouring O_C site. Based on this model for the photoexcited state, we can conclude that modification does not necessarily promote the spatial separation of photoexcited charges. However, both electrons and holes will be available at the modified surface for transfer to adsorbed species.

H_2O adsorption at Mn_4O_x-modified OH-rutile (110) and OH-anatase (101).

For the interaction of water at the modified surfaces, only those composites with O_V present were considered, as such vacancies are known to be active sites at metal oxide surfaces.[67; 90; 91; 92] Water adsorption is favourable at multiple sites of both modified surfaces and the geometries of the most stable adsorption configurations are displayed in Figure 4, while the *Supporting Information* shows other, less stable, water adsorption structures.

We adsorb water in molecular form at the heterostructures and relax the geometry. For Mn_4O_5-OH-r110, shown in Figure 4(a), water is adsorbed exothermically with a computed adsorption energy of -1.30 eV and spontaneously dissociates. Upon dissociation, an H atom migrates to a bridging O_S site and the water-derived hydroxyl (OH_W) is singly coordinated to an Mn site with an $Mn-O_W$ distance of 1.9 Å. The dissociation is accompanied by a transfer of charge from O_W to the nanocluster modifier, indicated by a decrease of 0.4 electrons in the computed Bader charge for the O_W ion. The Bader charges and spin magnetizations of cation sites are unchanged by the adsorption and dissociation. The moderate adsorption energy means that the hydroxyls should not be over-stabilized and could be active in catalysis.
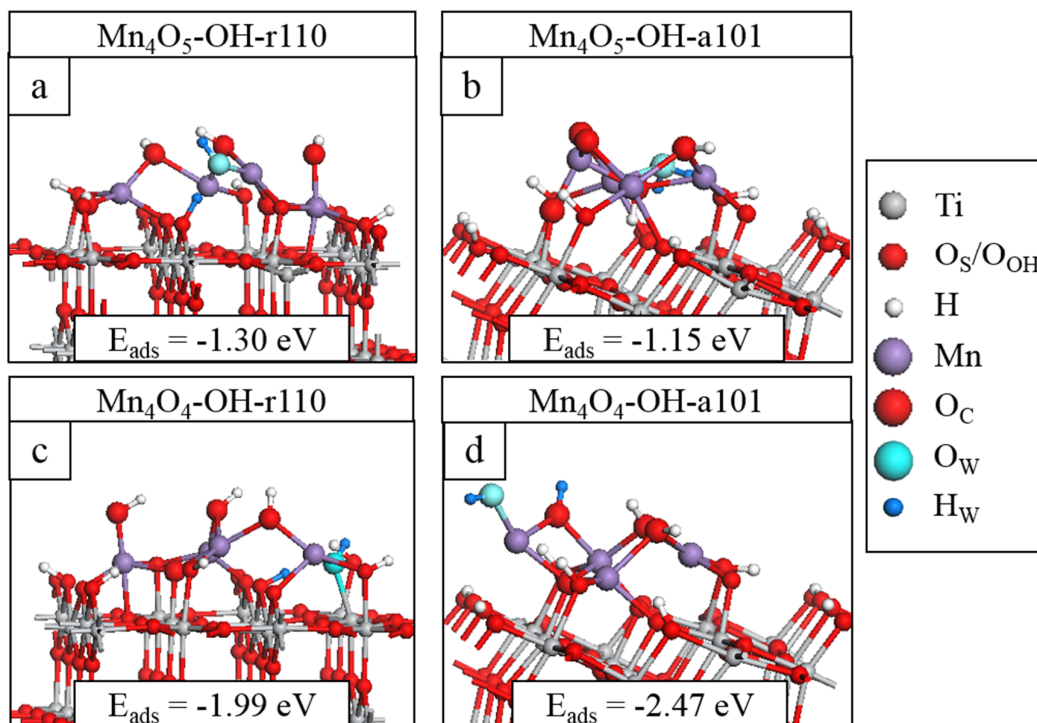
Figure 4 Relaxed atomic structures of the most stable configurations of H_2O adsorbed at **(a)** Mn_4O_5-OH-r110, **(b)** Mn_4O_5-OH-a101, **(c)** Mn_4O_4-OH-r110 and **(d)** Mn_4O_4-OH-a101. Atomic species are distinguished by colour according to the legend on the right hand side.

Water adsorbs molecularly at Mn_4O_5-OH-a101, as shown in Figure 4(b), with an adsorption energy of -1.15 eV. The H_2O binds to a single Mn ion with a $Mn-O_W$ distance of 2.2 Å. Since Mn_4O_5-OH-a101 is the ground state of this system, the single O_V having formed spontaneously, this composite favours non-stoichiometry and the strength of interaction with the water molecule is not sufficient to promote spontaneous dissociation.

The surfaces with two O_V show higher reactivity to water, as indicated by the larger adsorption energies in Figures 4(c) and (d). Water adsorbs and spontaneously dissociates at both Mn_4O_4-OH-r110 (Figure 4(c)) and Mn_4O_4-OH-a101 (Figure 4(d)). For Mn_4O_4-OH-r110, the water molecule adsorbs at an O_V site. An H atoms migrates to a bridging O_S site and the OH_W group is doubly coordinated to an Mn and a surface Ti site. Bader charge analysis reveals that 0.3

electrons are transferred from the O_W to the surface. The Ti ion which binds to OH_W was reduced to Ti^{3+}, due to O_V formation, prior to water adsorption and is re-oxidized to Ti^{4+}. This contrasts with work by Henderson *et al* in which no charge transfer was observed between Ti^{3+} and bridging hydroxyls bound at oxygen vacancy sites at the TiO_2 rutile (110) surface.[66] The reduced Ti site was only oxidised after interaction of O_2 with the Ti^{3+}-OH group. An Mn ion away from the adsorption site is reduced to Mn^{2+} so that after water dissociation at the surface there are three Mn^{2+} ions and one Ti^{3+}. The $Mn-O_W$ and $Ti-O_W$ distances are 2.2 Å.

For Mn_4O_4-OH-a101, the water molecule adsorbs at a two-fold coordinated Mn^{2+} ion and after dissociation an H atom migrates to an O_C ion which shows an increase in Bader charge, from 7.1 to 7.6 electrons. The Bader charges and spin magnetizations for cation sites are unchanged so that these ions are not involved in the charge transfer. The OH_W is singly coordinated to Mn with a $Mn-O_W$ distance of 1.9 Å.

Conclusions

The properties of Mn_4O_x-modified titania surfaces and their reduction and interaction with water depend on the phase of the TiO_2 substrate. For Mn_4O_6 adsorbed at the hydroxylated anatase (101) surface, interfacial bonds are established between cluster oxygen ions and the surface and Mn ions bind only to oxygen ions of the surface bound hydroxyls. Conversely, for Mn_4O_6 at hydroxylated rutile (110), the nanocluster-surface interaction is more intimate, with Mn ions binding to bridging and in-plane oxygen ions of the rutile surface.

Our results indicate that Mn_4O_x-OH-a101 favours non-stoichiometry as oxygen vacancies form spontaneously, whereas Mn_4O_x-OH-r110 is stoichiometric in the ground state. However, both composites can be considered highly reducible with moderate energy costs for oxygen vacancy

formation. Bader charge analysis shows that Mn ions are present in a mixture of oxidation states of at the hydroxylated anatase (101) surface, regardless of the stoichiometry. For Mn_4O_x-OH-rutile, both Mn and Ti ions are reduced in response to vacancy formation.

Modification with Mn_4O_x has a significant impact on the light absorption properties. Occupied Mn 3d states extend the VBM of the composites to higher energies relative to that of the titania support and empty states emerge below the CBM. The consequent red shift in the light absorption edge is confirmed by our model for the photoexcited state. The vertical energies, analogous to the optical energy gap, decrease significantly relative to those computed for the unmodified, hydroxylated rutile (110) and anatase (101) surfaces. Analysis of this model shows that electrons and holes localize at Mn and neighbouring O_C sites, respectively, so that modification may not promote separation of photoexcited charges but the trapping energies of the electron and hole are quite high, suggesting high stability.

With regard to water adsorption and activation, the formation of oxygen vacancies has an impact on the strength of interaction and the most favourable adsorption mode of H_2O at the modified surfaces. For Mn_4O_5-OH-a101, with a spontaneously formed O_V, water adsorbs only in molecular form. With formation of reducing oxygen vacancies, water adsorption becomes more exothermic and leads to spontaneous dissociation to surface bound hydroxyls, similar to observations made for water interacting at reduced TiO_2[66; 67] and CeO_2[68] surfaces.

21

resources at Tyndall Institute and the SFI/HEA funded Irish Centre for High End Computing.

We are grateful for support from the COST Action CM1104 "Reducible Metal Oxides, Structure and Function"

Conflicts of interest

None

References

[1] C. Jiang, S.J.A. Moniz, A. Wang, T. Zhang, and J. Tang, Photoelectrochemical devices for solar water splitting - materials and challenges. Chem. Soc. Rev. 46 (2017) 4645-4660.

[2] A. Fujishima, X. Zhang, and D.A. Tryk, TiO2 photocatalysis and related surface phenomena. Surf. Sci. Rep. 63 (2008) 515-582.

[3] M. Ni, M.K.H. Leung, D.Y.C. Leung, and K. Sumathy, A review and recent developments in photocatalytic water-splitting using TiO2 for hydrogen production. Renew. Sustainable Energy Rev. 11 (2007) 401-425.

[4] K. Maeda, and K. Domen, Photocatalytic Water Splitting: Recent Progress and Future Challenges. J. Phys. Chem. Lett. 1 (2010) 2655-2661.

[5] N.M. Dimitrijevic, B.K. Vijayan, O.G. Poluektov, T. Rajh, K.A. Gray, H. He, and P. Zapol, Role of Water and Carbonates in Photocatalytic Transformation of CO2 to CH4 on Titania. J. Am. Chem. Soc. 133 (2011) 3964-3971.

[6] S.N. Habisreutinger, L. Schmidt-Mende, and J.K. Stolarczyk, Photocatalytic Reduction of CO2 on TiO2 and Other Semiconductors. Angew. Chem. Int. Ed. 52 (2013) 7372-7408.

[7] M. Pelaez, N.T. Nolan, S.C. Pillai, M.K. Seery, P. Falaras, A.G. Kontos, P.S.M. Dunlop, J.W.J. Hamilton, J.A. Byrne, K. O'Shea, M.H. Entezari, and D.D. Dionysiou, A review on the visible light active titanium dioxide photocatalysts for environmental applications. Appl. Catal., B 125 (2012) 331-349.

[8] V. Etacheri, C. Di Valentin, J. Schneider, D. Bahnemann, and S.C. Pillai, Visible-light activation of TiO2 photocatalysts: Advances in theory and experiments. J. Photochem. Photobiol. C: Photochem. Rev. 25 (2015) 1-29.

[9] H. Tada, Q. Jin, A. Iwaszuk, and M. Nolan, Molecular-scale transition metal oxide nanocluster surface-modified titanium dioxide as solar-activated environmental catalysts. J. Phys. Chem. C 118 (2014) 12077-12086.

[10] A. Fujishima, and K. Honda, Electrochemical photolysis of water at a semiconductor electrode. Nature 238 (1972) 37-8.

[11] C. Di Valentin, E. Finazzi, G. Pacchioni, A. Selloni, S. Livraghi, M.C. Paganini, and E. Giamello, N-doped TiO2: Theory and experiment. Chem. Phys. 339 (2007) 44-56.

[12] X. Nie, S. Zhuo, G. Maeng, and K. Sohlberg, Doping of polymorphs for altered optical and photocatalytic properties. Int. J. Photoenergy 2009 (2009) 22.

[13] K. Yang, Y. Dai, B. Huang, and M.-H. Whangbo, Density functional characterization of the visible-light absorption in substitutional C-anion- and C-cation-doped TiO2. J. Phys. Chem. C 113 (2009) 2624-2629.

[14] J. Yu, Q. Xiang, and M. Zhou, Preparation, characterization and visible-light-driven photocatalytic activity of Fe-doped titania nanorods and first-principles study for electronic structures. Appl. Catal., B 90 (2009) 595-602.

[15] J.W. Zheng, A. Bhattcahrayya, P. Wu, Z. Chen, J. Highfield, Z. Dong, and R. Xu, The origin of visible light absorption in chalcogen element (S, Se, and Te)-doped anatase TiO2 photocatalysts. J. Phys. Chem. C 114 (2010) 7063-7069.

[16] A.M. Czoska, S. Livraghi, M. Chiesa, E. Giamello, S. Agnoli, G. Granozzi, E. Finazzi, C.D. Valentin, and G. Pacchioni, The nature of defects in fluorine-doped TiO2. J. Phys. Chem. C 112 (2008) 8951-8956.

[17] P. Haowei, L. Jingbo, L. Shu-Shen, and X. Jian-Bai, First-principles study of the electronic structures and magnetic properties of 3d transition metal-doped anatase TiO 2. J. Phys.: Condens. Matter 20 (2008) 125207.

[18] J.-M. Herrmann, Detrimental cationic doping of titania in photocatalysis: why chromium Cr3+-doping is a catastrophe for photocatalysis, both under UV- and visible irradiations. New J. Chem. 36 (2012) 883-890.

[19] T. Ikeda, T. Nomoto, K. Eda, Y. Mizutani, H. Kato, A. Kudo, and H. Onishi, Photoinduced dynamics of TiO2 doped with Cr and Sb. J. Phys. Chem. C 112 (2008) 1167-1173.

[20] J.-P. Xu, L. Li, L.-Y. Lv, X.-S. Zhang, X.-M. Chen, J.-F. Wang, F.-M. Zhang, W. Zhong, and Y.-W. Du, Structural and magnetic properties of Fe-doped anatase TiO 2 films annealed in vacuum. Chin. Phys. Lett. 26 (2009) 097502.

[21] W. Li, Influence of electronic structures of doped TiO2 on their photocatalysis. physica status solidi (RRL) – Rapid Research Letters 9 (2015) 10-27.

[22] S. Na Phattalung, S. Limpijumnong, and J. Yu, Passivated co-doping approach to bandgap narrowing of titanium dioxide with enhanced photocatalytic activity. Appl. Catal., B 200 (2017) 1-9.

[23] C.D. Valentin, G. Pacchioni, H. Onishi, and A. Kudo, Cr/Sb co-doped TiO2 from first principles calculations. Chem. Phys. Lett. 469 (2009) 166-171.

[24] Y. Gai, J. Li, S.S. Li, J.B. Xia, and S.H. Wei, Design of narrow-gap TiO2: a passivated codoping approach for enhanced photoelectrochemical activity. Phys. Rev. Lett. 102 (2009) 036402.

[25] R. Long, and N.J. English, First-principles calculation of synergistic (N, P)-codoping effects on the visible-light photocatalytic activity of anatase TiO2. J. Phys. Chem. C 114 (2010) 11984-11990.

[26] R. Long, and N.J. English, Synergistic effects on band gap-narrowing in titania by codoping from first-principles calculations. Chem. Mater. 22 (2010) 1616-1623.

[27] J. Zhang, C. Pan, P. Fang, J. Wei, and R. Xiong, Mo + C codoped TiO2 using thermal oxidation for enhancing photocatalytic activity. ACS Appl. Mater. Interfaces 2 (2010) 1173-1176.

[28] W. Zhu, X. Qiu, V. Iancu, X.-Q. Chen, H. Pan, W. Wang, N.M. Dimitrijevic, T. Rajh, H.M. Meyer, M.P. Paranthaman, G.M. Stocks, H.H. Weitering, B. Gu, G. Eres, and Z. Zhang, Band gap narrowing of titanium oxide semiconductors by noncompensated anion-cation codoping for enhanced visible-light photoactivity. Phys. Rev. Lett. 103 (2009) 226401.

[29] R. Chand, E. Obuchi, K. Katoh, H.N. Luitel, and K. Nakano, Enhanced photocatalytic activity of TiO2/SiO2 by the influence of Cu-doping under reducing calcination atmosphere. Catal. Commun. 13 (2011) 49-53.

[30] Y. Cui, H. Du, and L. Wen, Doped-TiO2 photocatalysts and synthesis methods to prepare TiO2 films. J. Mater. Sci. Technol. 24 (2008) 675-689.

[31] M. Guo, and J. Du, First-principles study of electronic structures and optical properties of Cu, Ag, and Au-doped anatase TiO2. Physica B: Condensed Matter 407 (2012) 1003-1007.

[32] H. Zhang, X. Yu, J.A. McLeod, and X. Sun, First-principles study of Cu-doping and oxygen vacancy effects on TiO2 for water splitting. Chem. Phys. Lett. 612 (2014) 106-110.

[33] D.O. Scanlon, C.W. Dunnill, J. Buckeridge, S.A. Shevlin, A.J. Logsdail, S.M. Woodley, C.R.A. Catlow, M.J. Powell, R.G. Palgrave, I.P. Parkin, G.W. Watson, T.W. Keal, P. Sherwood, A. Walsh, and A.A. Sokol, Band alignment of rutile and anatase TiO2. Nature Materials 12 (2013) 798.

[34] S.Y. Chae, C.S. Lee, H. Jung, O.-S. Joo, B.K. Min, J.H. Kim, and Y.J. Hwang, Insight into Charge Separation in WO3/BiVO4 Heterojunction for Solar Water Splitting. ACS Appl. Mater. Interfaces 9 (2017) 19780-19790.

[35] C. Sotelo-Vazquez, R. Quesada-Cabrera, M. Ling, D.O. Scanlon, A. Kafizas, P.K. Thakur, T.-L. Lee, A. Taylor, G.W. Watson, R.G. Palgrave, J.R. Durrant, C.S. Blackman, and I.P. Parkin, Evidence and Effect of Photogenerated Charge Transfer for Enhanced Photocatalysis in WO3/TiO2 Heterojunction Films: A Computational and Experimental Study. Adv. Funct. Mater. 27 (2017) 1605413.

[36] V.B.R. Boppana, and R.F. Lobo, SnOx–ZnGa2O4 Photocatalysts with Enhanced Visible Light Activity. ACS Catal. 1 (2011) 923-928.

[37] V.B.R. Boppana, F. Jiao, D. Newby, J. Laverock, K.E. Smith, J.C. Jumas, G. Hutchings, and R.F. Lobo, Analysis of visible-light-active Sn(ii)–TiO2 photocatalysts. Phys. Chem. Chem. Phys. 15 (2013) 6185-6189.

[38] J. Wang, H. Li, S. Meng, L. Zhang, X. Fu, and S. Chen, One-pot hydrothermal synthesis of highly efficient SnOx/Zn2SnO4 composite photocatalyst for the degradation of methyl orange and gaseous benzene. Appl. Catal., B 200 (2017) 19-30.

[39] S. Bhatia, and N. Verma, Photocatalytic activity of ZnO nanoparticles with optimization of defects. Mater. Res. Bull. 95 (2017) 468-476.

[40] T.R. Gordon, M. Cargnello, T. Paik, F. Mangolini, R.T. Weber, P. Fornasiero, and C.B. Murray, Nonaqueous Synthesis of TiO2 Nanocrystals Using TiF4 to Engineer Morphology, Oxygen Vacancy Concentration, and Photocatalytic Activity. J. Am. Chem. Soc. 134 (2012) 6751-6761.

[41] J. Zhang, I. Salles, S. Pering, P.J. Cameron, D. Mattia, and S. Eslava, Nanostructured WO3 photoanodes for efficient water splitting via anodisation in citric acid. RSC Advances 7 (2017) 35221-35227.

[42] C.B. Ong, L.Y. Ng, and A.W. Mohammad, A review of ZnO nanoparticles as solar photocatalysts: Synthesis, mechanisms and applications. Renew. Sustainable Energy Rev. 81 (2018) 536-551.

[43] Q. Jin, M. Fujishima, and H. Tada, Visible-light-active iron oxide-modified anatase titanium(iv) dioxide. J. Phys. Chem. C 115 (2011) 6478-6483.

[44] J.A. Libera, J.W. Elam, N.F. Sather, T. Rajh, and N.M. Dimitrijevic, Iron(iii)-oxo centers on TiO2 for visible-light photocatalysis. Chem. Mater. 22 (2010) 409-413.

[45] M. Nolan, Electronic coupling in iron oxide-modified TiO2 leads to a reduced band gap and charge separation for visible light active photocatalysis. Phys. Chem. Chem. Phys. 13 (2011) 18194-18199.

[46] M. Fronzi, A. Iwaszuk, A. Lucid, and M. Nolan, Metal oxide nanocluster-modified TiO 2 as solar activated photocatalyst materials. J. Phys.: Condens. Matter 28 (2016) 074006.

[47] A. Iwaszuk, M. Nolan, Q. Jin, M. Fujishima, and H. Tada, Origin of the visible-light response of nickel(ii) oxide cluster surface modified titanium(iv) dioxide. J. Phys. Chem. C 117 (2013) 2709-2718.

[48] Q. Jin, M. Fujishima, M. Nolan, A. Iwaszuk, and H. Tada, Photocatalytic activities of tin(iv) oxide surface-modified titanium(iv) dioxide show a strong sensitivity to the TiO2 crystal form. J. Phys. Chem. C 116 (2012) 12621-12626.

[49] D.S. Bhachu, S. Sathasivam, C.J. Carmalt, and I.P. Parkin, PbO-Modified TiO2 Thin Films: A Route to Visible Light Photocatalysts. Langmuir 30 (2014) 624-630.

[50] M. Nolan, A. Iwaszuk, and H. Tada, Molecular metal oxide cluster-surface modified titanium dioxide photocatalysts. Aust. J. Chem. 65 (2012) 624-632.

[51] J.B. Park, J. Graciani, J. Evans, D. Stacchiola, S. Ma, P. Liu, A. Nambu, J.F. Sanz, J. Hrbek, and J.A. Rodriguez, High catalytic activity of Au/CeOx/TiO2(110) controlled by the nature of the mixed-metal oxide at the nanometer level. Proceedings of the National Academy of Sciences 106 (2009) 4975-4980.

[52] J. Graciani, J.J. Plata, J.F. Sanz, P. Liu, and J.A. Rodriguez, A theoretical insight into the catalytic effect of a mixed-metal oxide at the nanometer level: The case of the highly active metal/CeOx/TiO2(110) catalysts. J. Chem. Phys. 132 (2010) 104703.

[53] S. Rhatigan, and M. Nolan, Impact of surface hydroxylation in MgO-/SnO-nanocluster modified TiO2 anatase (101) composites on visible light absorption, charge separation and reducibility. Chin. Chem. Lett. (2017).

[54] S. Rhatigan, and M. Nolan, CO2 and water activation on ceria nanocluster modified TiO2 rutile (110). J. Mater. Chem. A 6 (2018) 9139-9152.

[55] M. Nolan, Surface modification of TiO2 with metal oxide nanoclusters: a route to composite photocatalytic materials. Chem. Commun. 47 (2011) 8617-8619.

[56] M. Nolan, First-principles prediction of new photocatalyst materials with visible-light absorption and improved charge separation: surface modification of rutile TiO2 with nanoclusters of MgO and Ga2O3. ACS Appl. Mater. Interfaces 4 (2012) 5863-5871.

[57] A. Iwaszuk, and M. Nolan, Lead oxide-modified TiO2 photocatalyst: tuning light absorption and charge carrier separation by lead oxidation state. Catal. Sci. Technol. 3 (2013) 2000-2008.

[58] M. Nolan, A. Iwaszuk, and K.A. Gray, Localization of photoexcited electrons and holes on low coordinated Ti and O sites in free and supported TiO2 Nanoclusters. J. Phys. Chem. C 118 (2014) 27890-27900.

[59] A. Lucid, A. Iwaszuk, and M. Nolan, A first principles investigation of Bi2O3-modified TiO2 for visible light Activated photocatalysis: The role of TiO2 crystal form and the Bi3+ stereochemical lone pair. Mater. Sci. Semicond. Process. 25 (2014) 59-67.

[60] M. Fronzi, W. Daly, and M. Nolan, Reactivity of metal oxide nanocluster modified rutile and anatase TiO2: Oxygen vacancy formation and CO2 interaction. Applied Catalysis A: 521 (2016) 240-249.

[61] M. Nolan, Alkaline earth metal oxide nanocluster modification of rutile TiO2 (110) promotes water activation and CO2 chemisorption. J. Mater. Chem. A 6 (2018) 9451-9466.

[62] C.L. Muhich, B.D. Ehrhart, I. Al-Shankiti, B.J. Ward, C.B. Musgrave, and A.W. Weimer, A review and perspective of efficient hydrogen generation via solar thermal water splitting. Wiley Interdisciplinary Reviews: Energy and Environment 5 (2016) 261-287.

[63] M.V. Ganduglia-Pirovano, A. Hofmann, and J. Sauer, Oxygen vacancies in transition metal and rare earth oxides: Current state of understanding and remaining challenges. Surf. Sci. Rep. 62 (2007) 219-270.

[64] P. Mars, and D.W. van Krevelen, Oxidation Carried Out by Means of Vandium Oxide Catalysts, 1954.

[65] C. Di Valentin, and A. Selloni, Bulk and surface polarons in photoexcited anatase TiO2. J. Phys. Chem. Lett. 2 (2011) 2223-2228.

[66] M.A. Henderson, W.S. Epling, C.H.F. Peden, and C.L. Perkins, Insights into Photoexcited Electron Scavenging Processes on TiO2 Obtained from Studies of the Reaction of O2 with OH Groups Adsorbed at Electronic Defects on TiO2(110). J. Phys. Chem. B 107 (2003) 534-545.

[67] R. Schaub, P. Thostrup, N. Lopez, E. Lægsgaard, I. Stensgaard, J.K. Nørskov, and F. Besenbacher, Oxygen Vacancies as Active Sites for Water Dissociation on Rutile ${\mathrm{TiO}}_{2}(110)$. Phys. Rev. Lett. 87 (2001) 266104.

[68] D.R. Mullins, P.M. Albrecht, T.-L. Chen, F.C. Calaza, M.D. Biegalski, H.M. Christen, and S.H. Overbury, Water Dissociation on CeO2(100) and CeO2(111) Thin Films. J. Phys. Chem. C 116 (2012) 19419-19428.

[69] E. Lira, S. Wendt, P. Huo, J.Ø. Hansen, R. Streber, S. Porsgaard, Y. Wei, R. Bechstein, E. Lægsgaard, and F. Besenbacher, The Importance of Bulk Ti3+ Defects in the Oxygen Chemistry on Titania Surfaces. J. Am. Chem. Soc. 133 (2011) 6529-6532.

[70] L.-B. Xiong, J.-L. Li, B. Yang, and Y. Yu, Ti^{3+} in the Surface of Titanium Dioxide: Generation, Properties and Photocatalytic Application. Journal of Nanomaterials 2012 (2012) 13.

[71] Y. He, O. Dulub, H. Cheng, A. Selloni, and U. Diebold, Evidence for the Predominance of Subsurface Defects on Reduced Anatase ${\mathrm{TiO}}_{2}(101)$. Phys. Rev. Lett. 102 (2009) 106105.

[72] P. Scheiber, M. Fidler, O. Dulub, M. Schmid, U. Diebold, W. Hou, U. Aschauer, and A. Selloni, (Sub)Surface Mobility of Oxygen Vacancies at the ${\mathrm{TiO}}_{2}$ Anatase (101) Surface. Phys. Rev. Lett. 109 (2012) 136103.

[73] M. Setvin, U. Aschauer, J. Hulva, T. Simschitz, B. Daniel, M. Schmid, A. Selloni, and U. Diebold, Following the Reduction of Oxygen on TiO2 Anatase (101) Step by Step. J. Am. Chem. Soc. 138 (2016) 9565-9571.

[74] C. Franchini, R. Podloucky, J. Paier, M. Marsman, and G. Kresse, Ground-state properties of multivalent manganese oxides: Density functional and hybrid density functional calculations. Phys. Rev. B. 75 (2007) 195128.

[75] K.C. Schwartzenberg, J.W.J. Hamilton, A.K. Lucid, E. Weitz, J. Notestein, M. Nolan, J.A. Byrne, and K.A. Gray, Multifunctional photo/thermal catalysts for the reduction of carbon dioxide. Catal. Today 280 (2017) 65-73.

[76] G. Kresse, and J. Hafner, *Ab initio* molecular-dynamics simulation of the liquid-metal-amorphous-semiconductor transition in germanium. Phys. Rev. B. 49 (1994) 14251-14269.

[77] J. Furthmüller, J. Hafner, and G. Kresse, Dimer reconstruction and electronic surface states on clean and hydrogenated diamond (100) surfaces. Phys. Rev. B. 53 (1996) 7334-7351.

[78] P.E. Blöchl, Projector augmented-wave method. Phys. Rev. B. 50 (1994) 17953-17979.

[79] G. Kresse, and D. Joubert, From ultrasoft pseudopotentials to the projector augmented-wave method. Phys. Rev. B. 59 (1999) 1758-1775.

[80] J.P. Perdew, K. Burke, and M. Ernzerhof, Generalized gradient approximation made simple. Phys. Rev. Lett. 77 (1996) 3865-3868.

[81] M. Fronzi, and M. Nolan, Surface Modification of Perfect and Hydroxylated TiO2 Rutile (110) and Anatase (101) with Chromium Oxide Nanoclusters. ACS Omega 2 (2017) 6795-6808.

[82] V.I. Anisimov, J. Zaanen, and O.K. Andersen, Band theory and Mott insulators: Hubbard U instead of Stoner I. Phys. Rev. B. 44 (1991) 943-954.

[83] S.L. Dudarev, G.A. Botton, S.Y. Savrasov, C.J. Humphreys, and A.P. Sutton, Electron-energy-loss spectra and the structural stability of nickel oxide: An LSDA+U study. Phys. Rev. B. 57 (1998) 1505-1509.

[84] B.J. Morgan, and G.W. Watson, A DFT + U description of oxygen vacancies at the TiO2 rutile (1 1 0) surface. Surf. Sci. 601 (2007) 5034-5041.

[85] M. Nolan, S.D. Elliott, J.S. Mulley, R.A. Bennett, M. Basham, and P. Mulheran, Electronic structure of point defects in controlled self-doping of the ${\text{TiO}}_{2}$ (110) surface: Combined photoemission spectroscopy and density functional theory study. Phys. Rev. B. 77 (2008) 235424.

[86] A. Iwaszuk, and M. Nolan, Reactivity of sub 1 nm supported clusters: (TiO2)n clusters supported on rutile TiO2 (110). Phys. Chem. Chem. Phys. 13 (2011) 4963-4973.

[87] D.A. Kitchaev, H. Peng, Y. Liu, J. Sun, J.P. Perdew, and G. Ceder, Energetics of ${\mathrm{MnO}}_{2}$ polymorphs in density functional theory. Phys. Rev. B. 93 (2016) 045132.

[88] M. Nolan, A. Iwaszuk, A.K. Lucid, J.J. Carey, and M. Fronzi, Design of novel visible light active photocatalyst materials: surface modified TiO2. Adv. Mater. 28 (2016) 5425-5446.

[89] R.D. Shannon, and C.T. Prewitt, Effective ionic radii in oxides and fluorides. Acta Crystallographica Section B 25 (1969) 925-946.

[90] A. Ruiz Puigdollers, P. Schlexer, S. Tosoni, and G. Pacchioni, Increasing Oxide Reducibility: The Role of Metal/Oxide Interfaces in the Formation of Oxygen Vacancies. ACS Catal. 7 (2017) 6493-6513.

[91] F. Wang, S. Wei, Z. Zhang, G.R. Patzke, and Y. Zhou, Oxygen vacancies as active sites for H2S dissociation on the rutile TiO2(110) surface: a first-principles study. Phys. Chem. Chem. Phys. 18 (2016) 6706-6712.

[92] Y. Zhang, R. Dai, and S. Hu, Study of the role of oxygen vacancies as active sites in reduced graphene oxide-modified TiO2. Phys. Chem. Chem. Phys. 19 (2017) 7307-7315.